arXiv:0911.5690v1 [nlin.CD] 30 Nov 2009

A mechanism for switching near a heteroclinic network

Vivien Kirk, Department of Mathematics, University of Auckland,

Private Bag 92019, Auckland, New Zealand

Emily Lane, National Institute of Water and Atmospheric Research,

P O Box 8602, Christchurch, New Zealand

Claire M. Postlethwaite, Department of Mathematics, University of Auckland,

Private Bag 92019, Auckland, New Zealand

Alastair M. Rucklidge, Department of Applied Mathematics, University of Leeds,

Leeds LS2 9JT, UK

Mary Silber, Department of Engineering Sciences and Applied Mathematics,

Northwestern University, Evanston, IL 60208, USA

(November 30, 2009)

We describe an example of a structurally stable heteroclinic network for which nearby orbits exhibit irregular but sustained switching between the various sub-cycles in the network. The mechanism for switching is the presence of spiralling due to complex eigenvalues in the flow linearised about one of the equilibria common to all cycles in the network. We construct and use return maps to investigate the asymptotic stability of the network, and show that switching is ubiquitous near the network. Some of the unstable manifolds involved in the network are two-dimensional; we develop a technique to account for all trajectories on those manifolds. A simple numerical example illustrates the rich dynamics that can result from the interplay between the various cycles in the network.

1   Introduction

Heteroclinic cycles and networks are invariant sets that can occur in a struc-
turally stable way in systems with symmetry, and are known to provide a

v.kirk@auckland.ac.nz

e.lane@niwa.co.nz

c.postlethwaite@math.auckland.ac.nz

a.m.rucklidge@leeds.ac.uk

m-silber@northwestern.edu

2

robust mechanism for intermittent behaviour in these systems. For the purposes of this paper, we adopt the following definitions of heteroclinic cycles and heteroclinic networks. In the literature, there are more complicated definitions [6], but the simpler definitions presented here suffice for our purposes. For a finite-dimensional system of ordinary differential equations (ODEs), we define:

Definition. A *heteroclinic cycle* $\mathcal{C}$ is a finite collection of equilibria $\{\xi_1, \ldots, \xi_n\}$ of the ODEs, together with a set of heteroclinic connections $\{\gamma_1(t), \ldots, \gamma_n(t)\}$, where $\gamma_j(t)$ is a solution of the ODEs such that $\gamma_j(t) \to \xi_j$ as $t \to -\infty$ and $\gamma_j(t) \to \xi_{j+1}$ as $t \to \infty$, and where $\xi_{n+1} \equiv \xi_1$.

Definition. Let $\mathcal{C}_1, \mathcal{C}_2, \ldots$ be a collection of two or more heteroclinic cycles. We say that $\mathcal{N} = \bigcup_i \mathcal{C}_i$ forms a *heteroclinic network* if for each pair of equilibria in the network, there is a sequence of heteroclinic connections joining the equilibria. That is, for any $\xi_j, \xi_k \in \mathcal{N}$, we can find a sequence of heteroclinic connections $\{\gamma_{p_1}(t), \ldots, \gamma_{p_l}(t)\} \in \mathcal{N}$ and a sequence of equilibria $\{\xi_{m_1}, \ldots, \xi_{m_{l+1}}\} \in \mathcal{N}$ such that $\xi_{m_1} \equiv \xi_j$, $\xi_{m_{l+1}} \equiv \xi_k$ and γ_{p_i} is a heteroclinic connection between ξ_{m_i} and $\xi_{m_{i+1}}$.

Under this definition, a heteroclinic network is a connected collection of heteroclinic cycles, possibly infinite in number. We allow for an infinite number of cycles to co-exist in a network, as can occur, for instance, when one of the equilibria has a two-dimensional unstable manifold and there is a continuum of heteroclinic connections between that equilibrium and another. However, we restrict to the case where the set of all equilibria in the network is finite. In general, heteroclinic orbits can connect invariant sets other than equilibria, such as periodic orbits or chaotic saddles; we do not consider this possibility here.

Structurally stable heteroclinic cycles in symmetric systems have been studied extensively in recent years, with a canonical example arising in the context of rotating Rayleigh–Bénard convection [14] being analyzed in [19]. A good deal is now known about conditions for existence and stability of heteroclinic cycles (e.g., [9, 22, 24, 26]), and some results are also known about bifurcations of heteroclinic cycles and networks (e.g., [10, 16, 17, 31, 35]) and the effect on the dynamics of small symmetry breaking (e.g., [15, 20, 25, 27, 34]) or the addition of noise (e.g., [3, 12, 36]). Some experimental observations of near-heteroclinic cycles have been reported (e.g., see [28] for a recent example); experimental

noise and small symmetry-breaking effects prevent exact heteroclinic cycles from occurring, but near-heteroclinic structures are seen in certain regimes.

The dynamics near networks of heteroclinic cycles has been studied in, for instance, [1,5,13,17,21,30]. There are some natural questions to ask about the dynamics near heteroclinic networks. For example, is it the case that one cycle in the network is dominant, in that most trajectories near the network are attracted to that cycle, resulting in the network structure not being observed? Can more than one cycle be observed? Are there trajectories that switch between the cycles in the network in a sustained way, visiting all parts of the network eventually? Partial answers to these questions have been established.

Krupa and Melbourne [23] find conditions under which one cycle dominates in certain cases. However, their analysis does not cover the example of interest in this paper.

Kirk and Silber [21] construct an example where more than one cycle is observable, specifically showing that open sets of trajectories near the network may be attracted to each of the two primary cycles in their network. Despite both cycles being observable, there is no sustained switching in this example: an orbit may switch from one cycle to the other initially but may not switch back again. The effect of small noise on the network in [21] is studied in [3], where it is shown that noise can either induce switching of trajectories between cycles in the network or enhance the attractivity of certain cycles.

Aguiar et al. [1] describe an example, motivated by conjectures of Field [18], where trajectories switch between excursions about different cycles in a heteroclinic network. In this example some of the connections in the network result from transversal intersections between stable and unstable manifolds of equilibria, with the consequence that the network probably does not attract open sets of initial conditions. Because of the reinjection mechanisms built into the network, trajectories will make repeated passes near the transversal intersections and there are trajectories that follow arbitrarily complicated paths around the network, but these trajectories will not approach the network. Another example of this type is found in [2].

Postlethwaite and Dawes [30] examined an example of a heteroclinic network in which trajectories can exhibit periodic or aperiodic patterns of excursions past the various cycles in the network. The mechanism inducing switching between cycles in this network is a transverse instability of each cycle in one

4

direction. Almost all trajectories near a cycle eventually leave that cycle for another cycle, but that cycle in turn is unstable in a transverse direction and trajectories eventually leave that cycle too, ultimately returning to a neighbourhood of the original cycle. This mechanism operates when the network as a whole is essentially asymptotically stable, so trajectories get closer to the network as they cycle around the network.

Ashwin et al. [12] describe irregular switching near a heteroclinic network connecting periodic orbits and chaotic saddles confined to two invariant subspaces. In this case, the mechanism determining the switching is said to be nonlinear, since it appears to operate in a part of phase space well away from the invariant subspaces containing the periodic orbits and chaotic saddles. In this example, structurally stable connections again arise from transversal intersections of manifolds.

In this paper, we present another example in which orbits near a heteroclinic network switch repeatedly between excursions about the different cycles in the network. The mechanism for switching is the presence of a pair of complex eigenvalues in the linearisation of the flow about one of the equilibrium solutions in the network. Unlike the examples in Aguiar et al. [1, 2], where complex eigenvalues also occur, the heteroclinic connections in our network are structurally stable because of the symmetries of the problem and are non-transversal, with the consequence that, so long as symmetries are preserved, the network can attract open sets of initial conditions. As discussed further below, our example can exhibit an interesting form of switching, where the network structure is evident in the long term dynamics even though the network is not attracting. There are similarities between this and the switching observed in [1, 2], as discussed below.

The network we study is in $\mathbb{R}^4$ with $\mathbb{Z}_2^3$ symmetry, and is shown schematically in Figure 1. It consists of a set of six equilibria denoted A, B, X, Y, P and Q, their conjugate copies under action of the symmetries, and the set of heteroclinic connections joining the equilibria. Some of the heteroclinic connections occur in two-dimensional families, as indicated in Figure 1. There are many different heteroclinic cycles evident in Figure 1, e.g., $A \rightarrow B \rightarrow X \rightarrow A$ and $A \rightarrow B \rightarrow P \rightarrow X \rightarrow A$. The network is the union of all these cycles, and is described in more detail in section 2.

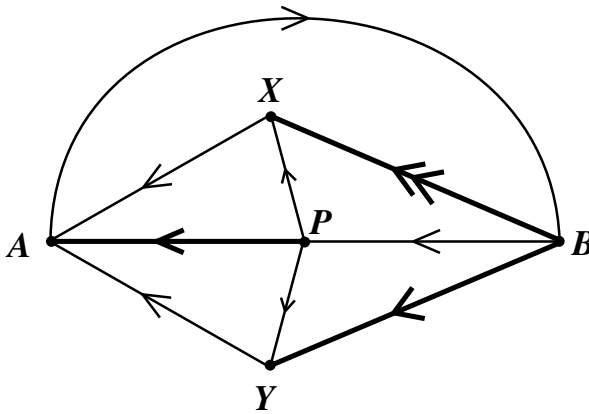Our analysis of this example proceeds in a standard way via construction

Figure 1.   Schematic diagram showing part of the heteroclinic network studied. For clarity, the equilibrium Q is not shown; this equilibrium plays a similar role to equilibrium P except that the one-dimensional heteroclinic connections from Q connect to $-X$ and Y instead of X and Y. The remaining (conjugate) parts of the network are obtained under the action of the $\mathbb{Z}_2^3$ symmetry group. The thin curves represent single heteroclinic connections while the bold curves indicate that a two-dimensional family of connections exists between the relevant equilibria. The double arrowhead on the connection from B to X indicates that expansion near B in the direction of this connection is stronger than the expansion in the direction of the connection from B to Y.

of return maps that approximate the dynamics in a neighbourhood of the heteroclinic network. A feature that complicates the construction is the existence of two-dimensional unstable manifolds of some of the equilibria in our network and hence of continua of heteroclinic connections between some pairs of equilibria. A novel aspect of our work is the way in which we allow for this complication; we have developed a relatively straightforward way to keep track of trajectories near two-dimensional unstable manifolds even when different orbits within a manifold connect different pairs of equilibria. The method is related to the technique used in [33] to analyze a homoclinic bifurcation in a problem with a two-dimensional unstable manifold, and it extends previous work on other problems with two-dimensional unstable manifolds such as [4, 5, 8, 9, 20].

Using these techniques, we are able to find a simple condition for asymptotic stability (resp., instability) of the network. The condition is as expected: the product of the ratio of contracting to expanding eigenvalues seen by a trajectory as it traverses the network must be greater than one (resp., less than one), regardless of the itinerary of the trajectory though the network. There is also an intermediate case, where whether there is net contraction or expansion

6

depends on the itinerary of the orbit past the various equilibria in the network. We go on to show that switching is ubiquitous in the network, whether or not the network is asymptotically stable. If the network is asymptotically stable, then we show that while orbits generically continue to switch as they approach the network, visits to certain equilibria become increasingly rare.

We find that a particularly interesting form of switching can occur in our network. If one of the cycles within the network attracts trajectories (i.e., a trajectory ends up closer to the network after making one passage near that cycle) while other cycles repel trajectories, then the net effect can be that a typical trajectory approaches an attractor (possibly chaotic) that lies near the network, with the trajectory repeatedly (but not uniformly) passing close to all parts of the network even though the network is not itself attracting. Under this scenario the network structure will be observed in the long term dynamics even though the network is not attracting. We report numerical observations of this form of switching, and defer a detailed investigation to a future paper.

The rest of this paper is organised as follows. §2 contains a description of our heteroclinic network and details of construction of the maps used to approximate the dynamics near the network. In §3 we find a condition for asymptotic stability of the network, and derive results about switching near the network. §4 gives results from numerical simulations of a system of four ordinary differential equations, illustrating the various switching phenomena associated with our example. Conclusions are contained in §5.

2   The heteroclinic network

We consider a system of ordinary differential equations, $\dot{\mathbf{x}} = \mathbf{f}(\mathbf{x})$, where $\mathbf{x} = (x_1, x_2, x_3, y_3) \in \mathbb{R}^4$ and $\mathbf{f} : \mathbb{R}^4 \to \mathbb{R}^4$ is a $\mathbf{C}^1$ vector-valued function. We assume this system is $\mathbb{Z}_2^3$-equivariant with the following equivariance properties:

$$\kappa_i(\mathbf{f}(\mathbf{x})) = \mathbf{f}(\kappa_i(\mathbf{x})), \qquad i = 1, 2, 3, \tag{1}$$

where

$$
\begin{aligned}
\kappa_1 : (x_1, x_2, x_3, y_3) &\rightarrow (-x_1, x_2, x_3, y_3), \\
\kappa_2 : (x_1, x_2, x_3, y_3) &\rightarrow (x_1, -x_2, x_3, y_3), \\
\kappa_3 : (x_1, x_2, x_3, y_3) &\rightarrow (x_1, x_2, -x_3, -y_3).
\end{aligned}
$$

These symmetries ensure the existence of dynamically invariant subspaces in which robust saddle–sink connections can occur. We make the following assumptions about the dynamics in these subspaces (see Figure 2).

- **A1**: There exist symmetry-related pairs of equilibria $\pm A$ and $\pm B$ on the x_1 and x_2 coordinate axes, respectively. Within the invariant plane $x_3 = y_3 = 0$, A is a saddle and B is a sink and there is a heteroclinic connection from A to B. See Figure 2(a).

- **A2:** There exist symmetry-related pairs of equilibria $\pm X$, $\pm Y$, $\pm P$ and $\pm Q$ in the invariant plane $x_1 = x_2 = 0$. Within this subspace, $\pm X$ and $\pm Y$ are sinks, while $\pm P$ and $\pm Q$ are saddles. The eight equilibria together with the heteroclinic connections between them make up an invariant curve C, which is topologically a circle. We hereafter refer to C as a circle, and we assume that C can be parametrised by the angle θ_3, the polar angle in the (x_3, y_3)-plane. Note that the intersections of the stable manifolds of $\pm P$ and $\pm Q$ with the invariant plane form the boundaries between the basins of attraction of $\pm X$ and $\pm Y$ in the invariant plane. Only a small part of each intersection is shown in Figure 2(b), to avoid giving a misleading impression about the dynamics near the origin of the (x_3, y_3)-plane, but each intersection curve in fact extends to the origin of the subspace.

- **A3:** Within the invariant subspace $x_1 = 0$, there exist two-dimensional manifolds of saddle–sink connections from B to $\pm X$ and $\pm Y$ (Figure 2(c)). There are also one-dimensional (saddle–saddle or saddle–sink) heteroclinic connections from B to $\pm P$ and $\pm Q$ and from $\pm P$ and $\pm Q$ to $\pm X$ and $\pm Y$, as shown in Figure 2(c). The unstable manifold of B is two-dimensional, and the stable manifolds of $\pm X$ and $\pm Y$ are each three-dimensional within the subspace.

- **A4:** Within the invariant subspace $x_2 = 0$, there exists a two-dimensional manifold of saddle–sink connections from $\pm X$, $\pm Y$, $\pm P$ and $\pm Q$ to A. Within this manifold, A is a stable focus. A similar manifold connects the
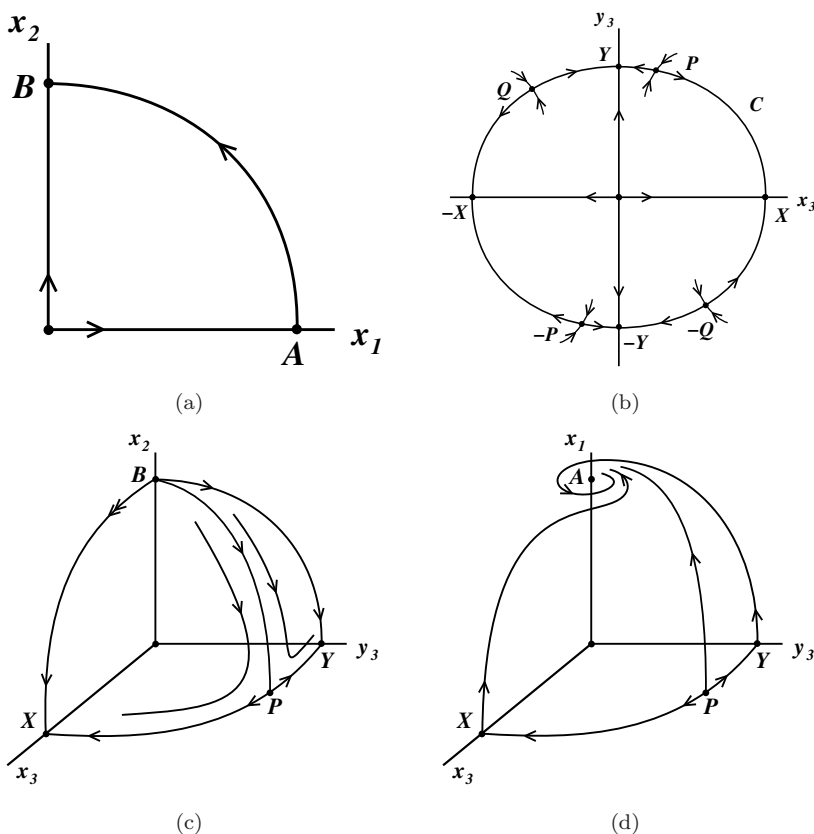
Figure 2.   Dynamics within the subspaces invariant under the symmetries κ_1, κ_2, κ_3 and their combinations. For clarity, only part of the relevant subspaces are shown in panels (a), (c) and (d), with the dynamics in the omitted parts being obtained by applying the symmetries. (a) The invariant plane $x_3 = y_3 = 0$, showing the heteroclinic connection from A to B. (b) The invariant plane $x_1 = x_2 = 0$, showing the invariant circle C and the equilibria $\pm X$, $\pm Y$, $\pm P$ and $\pm Q$ that lie on C. (c) The subspace $x_1 = 0$ showing part of the two-dimensional unstable manifold of B and part of the circle C in the (x_3, y_3) plane. Most trajectories leaving B go to either $\pm X$ or $\pm Y$, but some isolated trajectories go to $\pm P$ or $\pm Q$. For convenience, the equilibria $\pm X$ and $\pm Y$ are chosen to lie on the coordinate axes, with the eigenvectors of the corresponding linearised flow at B aligned with the axes, but they are not constrained by symmetry to be there. (d) The subspace $x_2 = 0$ showing spiralling of the unstable manifolds of X, Y and P into A. The unstable manifold of Q (not shown) behaves similarly. In each subspace, the flow is strongly contracting in the radial direction.

equilibria on C to $-A$. Apart from the heteroclinic connections from $\pm P$ and $\pm Q$ to $\pm X$ and $\pm Y$, the unstable manifolds of $\pm P$ and $\pm Q$ are contained in the stable manifolds of A and $-A$. There are no equilibria other than the origin and those mentioned above lying in the subspace $x_2 = 0$. See Figure 2(d).

- **A5:** Equilibrium B has real eigenvalues corresponding to dynamics in its unstable manifold, and these eigenvalues are unequal.

Assumptions **A1**−**A5** ensure the existence of the heteroclinic network shown in Figure 1. The symmetries κ_1 and κ_2 ensure that x_1 and x_2 cannot change sign along a trajectory, so we consider $x_1 \geq 0$ and $x_2 \geq 0$ only. The complex eigenvalues at A enable both signs of x_3 and y_3 to occur along trajectories. To simplify our analysis, we make the further assumptions:

- **A6:** At A and B, the directions of strongest contraction lie along the coordinate axes x_1 and x_2 respectively. At each of $\pm X$, $\pm Y$, $\pm P$ and $\pm Q$, the direction of strongest contraction lies in the (x_3, y_3) plane; this direction is automatically transverse to the connections from $\pm P$ or $\pm Q$ to $\pm X$ or $\pm Y$.
- **A7:** The two expanding eigenvectors at B lie in the x_3 and y_3 directions. Without loss of generality we assume that the eigenvalue in the x_3 direction is larger than that in the y_3 direction. We also assume that the linearisation around A, where there are complex eigenvalues, is in Jordan form.
- **A8:** The equilibria $\pm X$ and $\pm Y$ are, respectively, on the x_3 and y_3 coordinate axes.

Note that we can always choose coordinates so that at least one of **A7** and **A8** is satisfied, but we assume both are satisfied in order to simplify the calculations. This has no effect on our results.

Thus the overall network is $A \to B \to C \to A$, where, within C, trajectories can visit any of $\pm X$, $\pm Y$, $\pm P$ and $\pm Q$, although only in certain orders as indicated in Figures 1 and 2. All cycles in the network contain either three or four equilibria.

Definition. For a trajectory $\phi(t)$ close to the network, we define the *itinerary* of $\phi(t)$ to be the sequence $\{\xi_j\}$ of equilibria visited. That is, $\{\xi_j\}$ is the itinerary of the trajectory $\phi(t)$ if there exists an increasing sequence of times $\{t_j\}$ such that the distance from $\phi(t_j)$ to the equilibrium ξ_j is less than some small constant. For a trajectory that stays close to a single heteroclinic cycle, the itinerary will be a periodic sequence, with the (minimal) length of the repeating segment of the sequence being equal to the number of equilibria in the cycle.

In this paper we use the following definition for switching, defined for a particular trajectory close to a network. Note that Aguiar *et al.* [1] define switching as a property of a network, not individual trajectories.

Definition. We say a trajectory *switches* if, as $t \to \infty$, the itinerary is not eventually a periodic sequence with minimal period three or four, that is, the trajectory does not eventually remain near a single cycle of the network. In this definition, we distinguish between conjugate equilibria, that is, X and $-X$ and so on.

2.1   *Coordinates, cross-sections, and local maps*

In this section, we define the coordinates, cross-sections, and local maps required for modelling the dynamics near our heteroclinic network.

Near A and B, we define local coordinates that place the equilibrium at the origin. Assumption **A7** guarantees that the coordinate axes are aligned with the eigenvectors of the relevant linearised system. We use polar coordinates when it is more convenient: (x_3, y_3) becomes (r_3, θ_3), where $x_3 = r_3 \cos \theta_3$ and $y_3 = r_3 \sin \theta_3$. We write x_i or y_i if the local coordinate is the same as the corresponding global coordinate. At A and B we use u_1 and u_2 for the radial coordinate relative to the equilibrium points. At the invariant circle C, we use a θ_3-dependent coordinate transformation to define a radial coordinate u_3.

Near A, the linearised flow is given by:

$$\dot{u}_1 = -r_A u_1, \ \dot{x}_2 = e_A x_2, \ \dot{x}_3 = -c_A x_3 - \omega y_3, \ \dot{y}_3 = \omega x_3 - c_A y_3, \qquad (2)$$

where r_A, e_A, c_A and ω are positive constants. In polar coordinates, the $\dot{x}_3$ and $\dot{y}_3$ equations give $\dot{r}_3 = -c_A r_3$ and $\dot{\theta}_3 = \omega$.

Cross-sections near A are defined as:

$$\begin{aligned}
\mathbf{H}_A^{\text{in}} &\equiv \{(u_1, x_2, r_3, \theta_3) \,|\, |u_1| < h, 0 \leq x_2 < h, r_3 = h, 0 \leq \theta_3 < 2\pi\}, \\
\mathbf{H}_A^{\text{out}} &\equiv \{(u_1, x_2, r_3, \theta_3) \,|\, |u_1| < h, x_2 = h, 0 \leq r_3 < h, 0 \leq \theta_3 < 2\pi\}.
\end{aligned} \qquad (3)$$

Here $0 < h \ll 1$ is a parameter small enough that the cross-sections lie within the region of approximate linear flow near A (and similarly near B and C, as required below).

The flow near A induces a map $\phi_A : \mathbf{H}_A^{\text{in}} \to \mathbf{H}_A^{\text{out}}$, which is obtained to

lowest order by integrating equations (2):

$$\phi_A(u_1, x_2, h, \theta_3) = \left(u_1 \left(\frac{x_2}{h} \right)^{\frac{r_A}{e_A}}, h, h \left(\frac{x_2}{h} \right)^{\delta_A}, \theta_3 - \frac{\omega}{e_A} \log \left(\frac{x_2}{h} \right) \right) \quad (4)$$

where $\delta_A = \frac{c_A}{e_A}$.

Near B, the linearised flow is:

$$\dot{x}_1 = -c_B x_1, \;\; \dot{u}_2 = -r_B u_2, \;\; \dot{x}_3 = e_{Bx} x_3, \;\; \dot{y}_3 = e_{By} y_3, \quad (5)$$

where r_B, e_{Bx}, e_{By}, c_B are positive constants. From **A7**, we have $e_{Bx} > e_{By}$.

Cross-sections near B are defined as:

$$\begin{aligned}
\mathbf{H}_B^{\mathrm{in}} &\equiv \{(x_1, u_2, r_3, \theta_3) \,|\, x_1 = h, |u_2| < h, 0 \le r_3 < h, 0 \le \theta_3 < 2\pi\}, \\
\mathbf{H}_B^{\mathrm{out}} &\equiv \{(x_1, u_2, r_3, \theta_3) \,|\, 0 \le x_1 < h, |u_2| < h, r_3 = h, 0 \le \theta_3 < 2\pi\}.
\end{aligned} \quad (6)$$

The flow induces a map $\phi_B : \mathbf{H}_B^{\mathrm{in}} \to \mathbf{H}_B^{\mathrm{out}}$, which is obtained to lowest order by integrating equations (5). The map cannot be written down explicitly, but is computed as follows. First, the $\dot{x}_3$ and $\dot{y}_3$ equations are solved:

$$x_3(t) = r_3(0) \cos \theta_3(0) \, e^{e_{Bx} t}, \qquad y_3(t) = r_3(0) \sin \theta_3(0) \, e^{e_{By} t},$$

where $r_3(0)$ and $\theta_3(0)$ are the initial values of the radial coordinates (i.e., on $\mathbf{H}_B^{\mathrm{in}}$). The trajectory crosses $\mathbf{H}_B^{\mathrm{out}}$ when $r_3(t) = h$, so the transit time T_B is found by solving the equation

$$\left(\frac{h}{r_3(0)} \right)^2 = \cos^2 \theta_3(0) \, e^{2 e_{Bx} T_B} + \sin^2 \theta_3(0) \, e^{2 e_{By} T_B} \quad (7)$$

for T_B in terms of $r_3(0)$ and $\theta_3(0)$. This yields the local map $\phi_B : \mathbf{H}_B^{\mathrm{in}} \to \mathbf{H}_B^{\mathrm{out}}$:

$$\phi_B(h, u_2, r_3, \theta_3) = \left(h e^{-c_B T_B}, u_2 e^{-r_B T_B}, h, \tan^{-1} \left(\tan(\theta_3) e^{(e_{By} - e_{Bx}) T_B} \right) \right). \quad (8)$$

For later convenience, we define $\delta_{Bx} \equiv \delta_B^{\min} = \frac{c_B}{e_{Bx}}$ and $\delta_{By} \equiv \delta_B^{\max} = \frac{c_B}{e_{By}}$.

The treatment of the dynamics near the invariant circle C is more complicated. We assumed in **A2** that C can be parameterised by the angle θ_3. The rate of relaxation onto C is controlled by the θ_3-dependent eigenvalue $-r_C(\theta_3)$. The assumption of strong contraction in the radial (r_3) direction (**A6**) means

12

that the dynamics on C of θ_3 can be described by a one-dimensional nonlinear ODE of the form $\dot\theta_3 = g(\theta_3)$. The presence of $\pm X$ and $\pm Y$ on the coordinate axes will require $g(0) = g(\pi/2) = g(\pi) = g(3\pi/2) = 0$. The presence of $\pm P$ and $\pm Q$ will require further zeroes of g. This results in the flow near C being given by:

$$\dot x_1 = e_C(\theta_3)x_1, \ \dot x_2 = -c_C(\theta_3)x_2, \ \dot u_3 = -r_C(\theta_3)u_3, \ \dot\theta_3 = g(\theta_3), \qquad (9)$$

where r_C, e_C and c_C are positive functions of θ_3.

Cross-sections near C are defined as:

$$\begin{aligned}
\mathbf{H}_C^{\mathrm{in}} &\equiv \{(x_1, x_2, u_3, \theta_3) \,|\, 0 \le x_1 < h, x_2 = h, |u_3| < h, 0 \le \theta_3 < 2\pi\}, \\
\mathbf{H}_C^{\mathrm{out}} &\equiv \{(x_1, x_2, u_3, \theta_3) \,|\, x_1 = h, 0 \le x_2 < h, |u_3| < h, 0 \le \theta_3 < 2\pi\}.
\end{aligned} \qquad (10)$$

There is a continuum of heteroclinic connections from B to the various equilibrium points in C, and defining the cross-sections in this way allows us to keep track of all these connections.

The flow induces a map $\phi_C : \mathbf{H}_C^{\mathrm{in}} \to \mathbf{H}_C^{\mathrm{out}}$. As in the case of the flow past B, we cannot write down the map explicitly, but it is computed as follows. First, the $\dot\theta_3$ equation is solved using an initial condition $\theta_3(0)$, yielding $\theta_3(t)$. Then the $\dot x_1$ and $\dot x_2$ equations are solved:

$$x_1(t) = x_1(0) \exp\left(\int_0^t e_C(\theta_3(t'))\,dt'\right), \qquad x_2(t) = h \exp\left(-\int_0^t c_C(\theta_3(t'))\,dt'\right).$$

The trajectory crosses $\mathbf{H}_C^{\mathrm{out}}$ when $x_1(t) = h$, so the transit time T_C can be found in principle by solving

$$\int_0^{T_C} e_C(\theta_3(t'))\,dt' = -\log\left(\frac{x_1(0)}{h}\right) \qquad (11)$$

for T_C in terms of the initial values $x_1(0)$ and $\theta_3(0)$ on $\mathbf{H}_C^{\mathrm{in}}$. Then the local map $\phi_C : \mathbf{H}_C^{\mathrm{in}} \to \mathbf{H}_C^{\mathrm{out}}$ is given by

$$\phi_C(x_1, h, u_3, \theta_3) = \left(h, h \exp\left(-\int_0^{T_C} c_C(\theta_3(t'))\,dt'\right), u_3(T_C), \theta_3(T_C)\right), \quad (12)$$

where $u_3(T_C) = u_3 \exp\left(-\int_0^{T_C} r_C(\theta_3(t'))\,dt'\right)$. For later convenience, we define

δ_{CX}, δ_{CY}, δ_{CP} and δ_{CQ}, to be the ratio $\frac{c_C(\theta_3)}{e_C(\theta_3)}$ evaluated at the points X, Y, P and Q, respectively.

Neither of the local maps ϕ_B and ϕ_C can be written down explicitly. In the case of ϕ_B, the obstruction is only that we cannot write down an explicit solution of (7) for the transit time T_B. In the case of ϕ_C, the nonlinear evolution of θ_3 within C cannot be written down explicitly. However, in both cases, we will be able to give bounds on some properties of the trajectories, and this turns out to be sufficient for the purposes of determining stability and switching properties of the network.

2.2 *Global maps*

We construct global maps Ψ_{ij} to approximate the dynamics near the heteroclinic connections between A, B and C. In each case, we linearise the dynamics about the unstable manifold leaving the invariant set, taking into account the fact that the unstable manifold of A is one-dimensional, but the unstable manifolds of B and C are two-dimensional. We make use of the equivariance of the vector field in our map construction.

The simplest of the global maps is $\Psi_{AB} : \mathbf{H}_A^{\text{out}} \to \mathbf{H}_B^{\text{in}}$. The heteroclinic connection from A to B intersects $\mathbf{H}_A^{\text{out}}$ at $(u_1, x_2, x_3, y_3) = (0, h, 0, 0)$, and intersects $\mathbf{H}_B^{\text{in}}$ at $(x_1, u_2, x_3, y_3) = (h, \epsilon_B, 0, 0)$, for a small constant ϵ_B. Generically, $\epsilon_B \neq 0$ and we assume that this is the case in the following. Near the heteroclinic connection the map expressed in cartesian coordinates is at lowest order an affine linear transformation. Converting to polar coordinates, this yields, at leading order:

$$\Psi_{AB}(u_1, h, r_3, \theta_3) = (h, \epsilon_B, D_B(\theta_3)r_3, \bar{\theta}_B(\theta_3)), \tag{13}$$

where $D_B(\theta_3)$ is an order-one function of θ_3 that indicates how the small variable r_3 is scaled in the transition from A to B, and $\bar{\theta}_B(\theta_3)$ is an order-one function of θ_3. The invariance of this map under the symmetry κ_3 ensures that there is no constant term in the r_3 component. The overall effect of this map is to multiply r_3 by an order-one amount D_B, and to rigidly rotate the angle θ_3.

The unstable manifold of B is two-dimensional; it intersects $\mathbf{H}_B^{\text{out}}$ at $(x_1, u_2, r_3, \theta_3) = (0, 0, h, \theta_3)$, for $0 \leq \theta_3 < 2\pi$, and it intersects $\mathbf{H}_C^{\text{in}}$ at

14

$(x_1, x_2, u_3, \theta_3) = (0, h, \epsilon_C(\theta_3), \bar{\theta}_C(\theta_3))$, where ϵ_C is a small function of θ_3 and $\bar{\theta}_C$ is an order-one function of θ_3. For small x_1 and u_2, we have at leading order:

$$\Psi_{BC}(x_1, u_2, h, \theta_3) = \left(D_C(\theta_3)x_1, h, \epsilon_C(\theta_3), \bar{\theta}_C(\theta_3)\right), \qquad (14)$$

where $D_C(\theta_3)$ is an order-one function of θ_3. Here $\epsilon_C(\theta_3)$ plays a similar role to the constant ϵ_B in (13), except that it takes on a different constant value for each heteroclinic connection and so is a function of θ_3. As with ϵ_B, $\epsilon_C(\theta_3)$ is generically non-zero and we assume that $\epsilon_C(\theta_3) \neq 0$ for any θ_3.

The effect of (14) is to multiply the small variable x_1 by an order-one function of θ_3, and to map the outgoing angle θ_3 to an incoming angle $\bar{\theta}_C$. Unlike in the case of Ψ_{AB}, the effect of $\bar{\theta}_C$ need not be a rotation.

For the global map $\Psi_{CA} : \mathbf{H}_C^{\text{out}} \rightarrow \mathbf{H}_A^{\text{in}}$, we also use (r_3, θ_3) rather than (x_3, y_3). The unstable manifold of C is two-dimensional; it intersects $\mathbf{H}_C^{\text{out}}$ at $(x_1, x_2, u_3, \theta_3) = (h, 0, 0, \theta_3)$, where $0 \leq \theta_3 < 2\pi$, and it intersects $\mathbf{H}_A^{\text{in}}$ at $(u_1, x_2, r_3, \theta_3) = (\epsilon_A(\theta_3), 0, h, \bar{\theta}_A(\theta_3))$, where ϵ_A is a small function of θ_3, and $\bar{\theta}_A$ is an order-one function of θ_3. For small x_2 and u_3, we have:

$$\Psi_{CA}(h, x_2, u_3, \theta_3) = \left(\epsilon_A(\theta_3), D_A(\theta_3)x_2, h, \bar{\theta}_A(\theta_3)\right), \qquad (15)$$

where $D_A(\theta_3)$ is an order-one function of θ_3. The effect of this map is to multiply the small variable x_2 by an order-one function of θ_3, and to map the outgoing angle θ_3 to an incoming angle $\bar{\theta}_A$. As in the case of Ψ_{BC}, the effect of $\bar{\theta}_A$ need not be a rotation.

3   Analysis of the maps

By composing the local and global maps in an appropriate order, we construct return maps that approximate the dynamics near the cycles in our network. We are interested in finding conditions under which the network as a whole is attracting, and in describing the switching properties of trajectories as they travel around the network. We are particularly interested in trajectories that repeatedly visit both X (or $-X$) and Y (or $-Y$).

In our analysis, as in [20], we make use of the observation that at each cross-

section, the four variables play distinct roles. Two variables are unimportant: the one that is equal to h, and the one in the radial direction. Of the other two variables, one is *small* and measures the distance from an invariant subspace, and the other is the order-one *angle* θ_3. At each cross-section, the roles change, but there are always small and angle variables.

3.1   *Stability results*

To show that the network as a whole is attracting, we must find conditions under which the small variable decreases each time around the network. In order to do this, we bound this variable over all possible values of the angle variable. This means that we need to take into account the details of which part of C is visited by the trajectory. We are unable to compute the stability result by direct computation of a return map, since the local maps ϕ_B and ϕ_C are only known implicitly, but the lengthy computation below achieves the same result.

We start on $\mathbf{H}_A^{\text{in}}$ at (u_1, x_2, h, θ_3), and consider the effects of maps ϕ_A, Ψ_{AB}, ϕ_B, Ψ_{BC}, ϕ_C and Ψ_{CA} in turn. We assume that $x_2 \ll 1$. After ϕ_A and Ψ_{AB}, we arrive on $\mathbf{H}_B^{\text{in}}$ at:

$$
\left(h, \epsilon_B, hD_B\left(\theta_3 - \frac{\omega}{e_A} \log\left(\frac{x_2}{h} \right) \right) \left(\frac{x_2}{h} \right)^{\delta_A}, \bar{\theta}_B\left(\theta_3 - \frac{\omega}{e_A} \log\left(\frac{x_2}{h} \right) \right) \right),
$$

where we have discarded all higher-order corrections. For convenience, we label the values of r_3 and θ_3 on $\mathbf{H}_B^{\text{in}}$ as $r_3^{(B_{\text{in}})}$ and $\theta_3^{(B_{\text{in}})}$, with a similar convention on other cross-sections. We define $D_B^{\max}$ and $D_B^{\min}$ to be the maximum and minimum values of D_B taken over all values of θ_3. Then we can bound the small variable $r_3^{(B_{\text{in}})}$ by

$$
hD_B^{\min}\left(\frac{x_2}{h} \right)^{\delta_A} \leq r_3^{(B_{\text{in}})} \leq hD_B^{\max}\left(\frac{x_2}{h} \right)^{\delta_A}. \tag{16}
$$

Next, we consider the effect of maps ϕ_B and Ψ_{BC}. Recall from (**A7**) that $e_{Bx} > e_{By}$. From (7) we can bound T_B:

$$
-\frac{1}{e_{Bx}} \log\left(\frac{r_3^{(B_{\text{in}})}}{h} \right) \leq T_B \leq -\frac{1}{e_{By}} \log\left(\frac{r_3^{(B_{\text{in}})}}{h} \right).
$$

16

As a result, the small variable $x_1^{(B_{\text{out}})}$ on $\mathbf{H}_B^{\text{out}}$ is bounded by

$$h \left(\frac{r_3^{(B_{\text{in}})}}{h} \right)^{\delta_{By}} \leq x_1^{(B_{\text{out}})} \leq h \left(\frac{r_3^{(B_{\text{in}})}}{h} \right)^{\delta_{Bx}} .$$

Note that $\delta_{Bx} < \delta_{By}$. After Ψ_{BC}, trajectories enter $\mathbf{H}_C^{\text{in}}$ at:

$$\left(D_C \left(\theta_3^{(B_{\text{out}})} \right) x_1^{(B_{\text{out}})}, h, \epsilon_C(\theta_3), \bar{\theta}_C \left(\theta_3^{(B_{\text{out}})} \right) \right),$$

where we have discarded all higher-order corrections. We define $D_C^{\max}$ and $D_C^{\min}$ to be the maximum and minimum values of D_C taken over all values of θ_3. Then we can bound $x_1^{(C_{\text{in}})}$ by

$$h D_C^{\min} \left(\frac{r_3^{(B_{\text{in}})}}{h} \right)^{\delta_{By}} \leq x_1^{(C_{\text{in}})} \leq h D_C^{\max} \left(\frac{r_3^{(B_{\text{in}})}}{h} \right)^{\delta_{Bx}} . \tag{17}$$

Finally, we consider the effects of maps ϕ_C and Ψ_{CA}. The first of these is the most complicated as trajectories can enter the neighbourhood of C close to any of the equilibrium points $\pm X$, $\pm Y$, $\pm P$ or $\pm Q$ (or in between), and can similarly exit the neighbourhood of C close to any of the equilibrium points $\pm X$, $\pm Y$, $\pm P$ or $\pm Q$ (or in between). We take all possibilities into account and derive a bound on the exit value of the small variable x_2.

To simplify the discussion, we consider in detail only the case of trajectories arriving at C between X and P; the other cases can easily be deduced from this one. Within C, X is stable, with a stable eigenvalue $-\lambda_X$, and P is unstable, with an unstable eigenvalue λ_P, with $\lambda_X, \lambda_P > 0$. The corresponding eigenvectors are within the (x_3, y_3) plane, and are tangent to C at X and P. To aid the analysis, we consider cross-sections orthogonal to C, at $\theta_3 = \theta_3^X + h$ and $\theta_3 = \theta_3^P - h$, where θ_3^X and θ_3^P are the θ_3 coordinates of X and P respectively, and h is as before (see Figure 3). Note that we have defined our coordinates so that $\theta_3^X = 0$, but for clarity of the following discussion we leave this constant in symbolic form.

There are three main possibilities, indicated in Figure 3: (a) the trajectory crosses $\mathbf{H}_C^{\text{in}}$ near X and must therefore cross $\mathbf{H}_C^{\text{out}}$ near X as well; (b) the trajectory crosses $\mathbf{H}_C^{\text{in}}$ near P and also crosses $\mathbf{H}_C^{\text{out}}$ near P; and (c) the trajectory crosses $\mathbf{H}_C^{\text{in}}$ near P and leaves the neighbourhood of P, heading towards X,
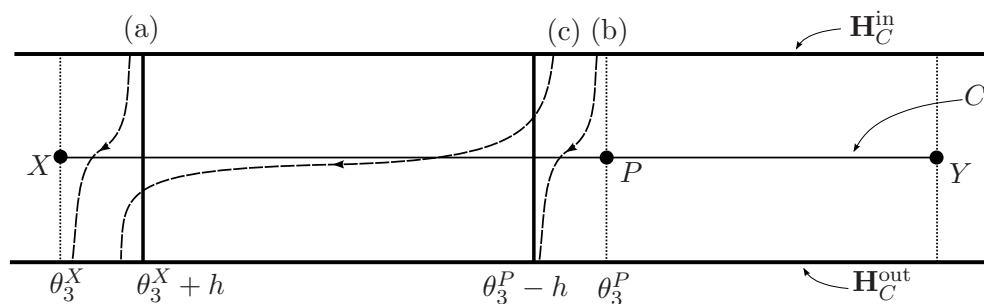
Figure 3. Schematic showing three main possibilities of how trajectories pass through the region near C. Trajectories are shown as dashed lines, Poincaré sections as solid bold lines. Equilibria are indicated by dots. The labels (a), (b) and (c) identify trajectories representative of three cases discussed in the text.

and so crosses $\mathbf{H}_C^{\mathrm{out}}$ near X. There are the additional possibilities that the trajectory crosses $\mathbf{H}_C^{\mathrm{in}}$ or $\mathbf{H}_C^{\mathrm{out}}$ in between X and P; we discuss these cases below. Throughout this discussion, we disregard the radial coordinate r_3.

Case (a) is straightforward: the flow near X is given by the linearisation of (9) around X:

$$\dot{x}_1 = e_C(\theta_3^X)x_1, \ \dot{x}_2 = -c_C(\theta_3^X)x_2, \ \dot{\theta}_3 = -\lambda_X(\theta_3 - \theta_3^X), \tag{18}$$

and so the linearised map near X takes an incoming point $(x_1^{(C_{\mathrm{in}})}, h, \theta_3^{(C_{\mathrm{in}})})$ to

$$(x_1, x_2^{(C_{\mathrm{out}})}, \theta_3^{(C_{\mathrm{out}})}) = \left(h, h\left(\frac{x_1^{(C_{\mathrm{in}})}}{h}\right)^{\delta_{CX}}, \theta_3^X + (\theta_3^{(C_{\mathrm{in}})} - \theta_3^X)\left(\frac{x_1^{(C_{\mathrm{in}})}}{h}\right)^{\frac{\lambda_X}{e_C(\theta_3^X)}} \right),$$

where δ_{CX} is the ratio of contracting to expanding eigenvalues evaluated at X.

Similarly, case (b) is treated by linearising (9) around P, and results in exit values

$$(x_1, x_2^{(C_{\mathrm{out}})}, \theta_3^{(C_{\mathrm{out}})}) = \left(h, h\left(\frac{x_1^{(C_{\mathrm{in}})}}{h}\right)^{\delta_{CP}}, \theta_3^P + (\theta_3^{(C_{\mathrm{in}})} - \theta_3^P)\left(\frac{x_1^{(C_{\mathrm{in}})}}{h}\right)^{\frac{-\lambda_P}{e_C(\theta_3^P)}} \right),$$

where $\delta_{CP} = \frac{c_C(\theta_3^P)}{e_C(\theta_3^P)}$ is the ratio of contracting to expanding eigenvalues evaluated at P. The condition that the trajectory crosses $\mathbf{H}_C^{\mathrm{out}}$ before it crosses

$\theta_3 = \theta_3^P - h$ amounts to:

$$\left|\theta_3^{(C_{\text{in}})} - \theta_3^P\right| \left(\frac{x_1^{(C_{\text{in}})}}{h}\right)^{\frac{-\lambda_P}{e_C(\theta_3^P)}} < h,$$

that is, the trajectory must enter C close enough to P that the small variable x_1 grows to size h before the angular separation $\theta_3 - \theta_3^P$ grows to size h.

Finally, in case (c), there are three stages: linearised dynamics near P, a jump from P to X, and linearised dynamics near X. The time for the first stage is found by setting $\theta_3(t) = \theta_3^P - h$, and then the (x_1, x_2) coordinates on this section are:

$$\left(x_1^{(C_{\text{in}})} \left|\frac{\theta_3^{(C_{\text{in}})} - \theta_3^P}{h}\right|^{-\frac{e_C(\theta_3^P)}{\lambda_P}} , h\left|\frac{\theta_3^{(C_{\text{in}})} - \theta_3^P}{h}\right|^{\frac{c_C(\theta_3^P)}{\lambda_P}}\right).$$

Then there is a jump from $\theta_3 = \theta_3^P - h$ to $\theta_3 = \theta_3^X + h$, during which x_1 and x_2 change by a factor of $D_{X,1}$ and $D_{X,2}$ respectively. The values of $D_{X,1}$ and $D_{X,2}$ depend on h. Lastly, there is the linearised dynamics near X, which results in an exit value of x_2 given by:

$$x_2^{(C_{\text{out}})} = h D_{X,2} \left(\frac{D_{X,1} x_1^{(C_{\text{in}})}}{h}\right)^{\delta_{CX}} \left|\frac{\theta_3^{(C_{\text{in}})} - \theta_3^P}{h}\right|^{\frac{e_C(\theta_3^P)}{\lambda_P}(\delta_{CP} - \delta_{CX})}. \qquad (19)$$

This case only occurs if

$$\left|\frac{\theta_3^{(C_{\text{in}})} - \theta_3^P}{h}\right|^{\frac{e_C(\theta_3^P)}{\lambda_P}} > \frac{x_1^{(C_{\text{in}})}}{h} \qquad (20)$$

(otherwise we would be in case (b)). This condition allows us to bound the exit values of x_2. Note first that $\left|\frac{\theta_3^{(C_{\text{in}})} - \theta_3^P}{h}\right|^{\frac{e_C(\theta_3^P)}{\lambda_P}} < 1$. Then if $\delta_{CP} > \delta_{CX}$, from (19) we have that $x_2^{(C_{\text{out}})}$ is bounded above by a constant times $\left(x_1^{(C_{\text{in}})}\right)^{\delta_{CX}}$. Additionally, using (20) in (19), we have that $x_2^{(C_{\text{out}})}$ is bounded below by a constant times $\left(x_1^{(C_{\text{in}})}\right)^{\delta_{CP}}$. Similar considerations in the case that $\delta_{CP} < \delta_{CX}$

give additional constraints which altogether result in:

$$
hD_X^{\min} \left(\frac{x_1^{(C_{\mathrm{in}})}}{h} \right)^{\max(\delta_{CP}, \delta_{CX})} \leq x_2^{(C_{\mathrm{out}})} \leq hD_X^{\max} \left(\frac{x_1^{(C_{\mathrm{in}})}}{h} \right)^{\min(\delta_{CP}, \delta_{CX})} ,
$$

where $D_X^{\min}$ and $D_X^{\max}$ are constants that depend on $D_{X,1}$ and $D_{X,2}$ and some exponents.

The same analysis can be used in the cases where trajectories enter or leave the neighbourhood of C in between the neighbourhoods of P and X, with only minor alterations of the values of the constants $D_X^{\min}$ and $D_X^{\max}$. Then all possibilities (a), (b) and (c) can be assembled, as well as including trajectories that visit the equilibria Y and Q as well, and the map Ψ_{CA} can be applied. All this results in a bound on the value of $x_2^{(A_{\mathrm{in}})}$ at $\mathbf{H}_A^{\mathrm{in}}$ of the form:

$$
hD_A^{\min} \left(\frac{x_1^{(C_{\mathrm{in}})}}{h} \right)^{\delta_C^{\max}} \leq x_2^{(A_{\mathrm{in}})} \leq hD_A^{\max} \left(\frac{x_1^{(C_{\mathrm{in}})}}{h} \right)^{\delta_C^{\min}} , \tag{21}
$$

where we interpret $\delta_C^{\max}$ as $\max(\delta_{CX}, \delta_{CY}, \delta_{CP}, \delta_{CQ})$, and similarly $\delta_C^{\min}$, and the constants $D_A^{\min}$ and $D_A^{\max}$ are the smallest and largest of all the constants in the local and global parts of the maps.

Recall that the trajectory started on $\mathbf{H}_A^{\mathrm{in}}$ with particular values of x_2 and θ_3. In computing these bounds, the value of θ_3 has been lost, but inequalities (16), (17) and (21) provide the smallest and largest possible values of x_2 once the trajectory returns to $\mathbf{H}_A^{\mathrm{in}}$:

$$
hD_{ABC}^{\min} \left(\frac{x_2}{h} \right)^{\delta^{\max}} \leq x_2^{(A_{\mathrm{in}})} \leq hD_{ABC}^{\max} \left(\frac{x_2}{h} \right)^{\delta^{\min}} . \tag{22}
$$

Here $\delta^{\max} = \delta_A \delta_B^{\max} \delta_C^{\max}$, $\delta^{\min} = \delta_A \delta_B^{\min} \delta_C^{\min}$, and all the constants have been amalgamated into $D_{ABC}^{\min}$ and $D_{ABC}^{\max}$.

We have thus established a condition for asymptotic stability or instability of the network. If $\delta^{\min} > 1$, then a trajectory starting close enough to the network will return closer to the network (with a smaller value of x_2) regardless of which itinerary it takes and regardless of the values of $D_{ABC}^{\min}$ and $D_{ABC}^{\max}$, and so the network is asymptotically stable. If $\delta^{\max} < 1$, then a trajectory starting close to the network will return further away from the network (with a larger value

of x_2) regardless of which itinerary it takes, and so the network is unstable. The values of the constants can be scaled away in both these cases.

These conditions for asymptotically stability and instability are as expected: the product of the ratio of the contracting to expanding eigenvalues should be greater or less than one regardless of the itinerary. The more interesting and complicated case is when $\delta^{\min} < 1 < \delta^{\max}$, in which case it appears that whether there is net contraction or expansion depends on the itinerary. We present some numerical results relevant to this case in section 4. These results suggest that the network may be essentially asymptotically stable or unstable, depending on which of the routes through the network is responsible for $\delta^{\max} > 1$ and which is responsible for $\delta^{\min} < 1$.

3.2 *Switching near the network*

In this section, we show that close enough to the network, there are trajectories that, over the course of two circuits around the network, visit any combination of the equilibrium points within C in any order. This occurs whether or not the network is asymptotically stable. We also show that when the network is asymptotically stable, most trajectories repeatedly visit both X and $-X$ as they approach the network. On the assumption that the complex eigenvalues at A mix trajectories effectively, we estimate how often trajectories visit $\pm Y$ and show that, when the network is asymptotically stable, visits to $\pm Y$ become rare as trajectories approach the network. Finally, we show that interesting switching dynamics might be possible in the case $\delta^{\min} < 1 < \delta^{\max}$, when some parts of the network are attracting and other parts are repelling.

Figure 4 shows schematically how trajectories visit different parts of C, according to where they cross $\mathbf{H}_B^{\text{in}}$. The majority of trajectories go to X or $-X$, and there are cusp-shaped regions that visit P then X, P only, etc., on their way to A.

Consider a line segment of initial conditions on $\mathbf{H}_B^{\text{in}}$, with a fixed value of θ_3 and a range of values of r_3: $0 < r_3^a \leq r_3 \leq r_3^b < h$ (see Figure 5). We choose θ_3 such that the family of trajectories first travels around the network via the point X. We will show that the spread of r_3 values translates into a spread of θ_3 values once the line segment has been mapped around the network. This arises in particular from the complex eigenvalues at A. We can choose the
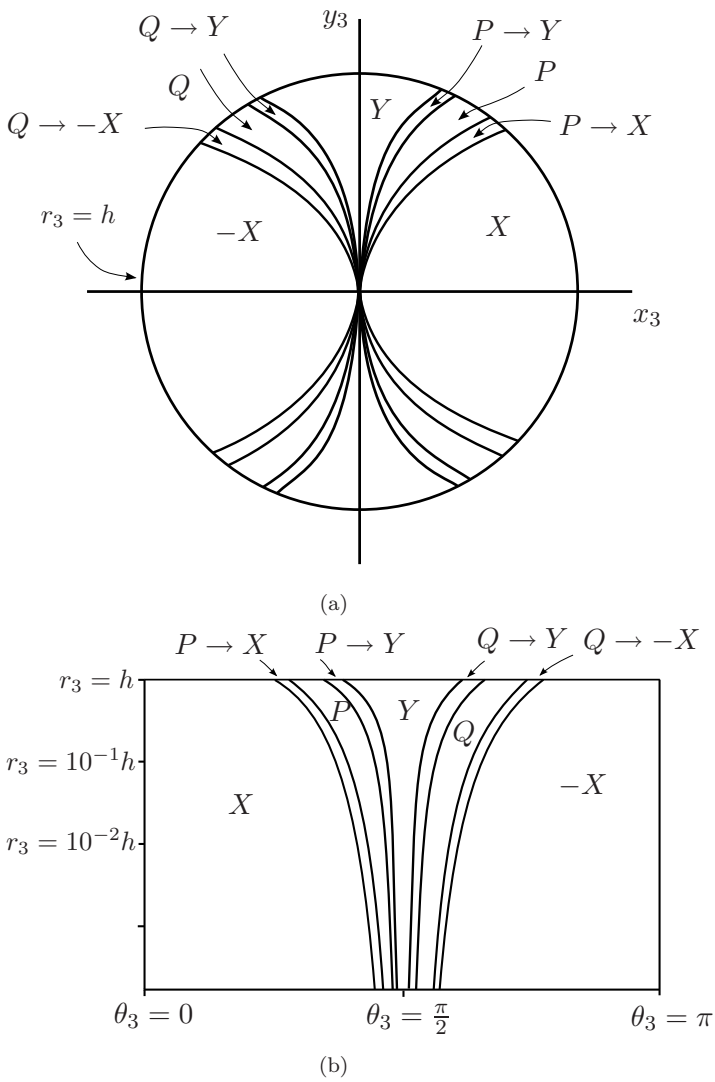
(a)

(b)

Figure 4. Schematic diagram showing a slice (with constant u_2) of the Poincaré section $\mathbf{H}_B^{\text{in}}$, using (a) Cartesian and (b) logarithmic polar coordinates. Only part of the slice in (a) is shown in (b). Each slice is divided into regions according to the equilibrium in C visited by the trajectories in that region as they pass from B to A.

values of r_3^a and r_3^b such that after one cycle around the network, the line segment covers $\theta_3 \in [0, 2\pi]$. This means that there are trajectories with initial conditions in the initial segment that visit each of the different parts of C on the second time around the network.
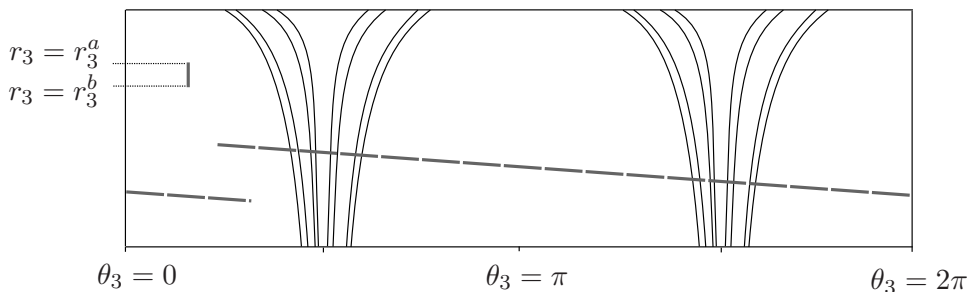
22

$$r_3 = r_3^a$$
$$r_3 = r_3^b$$

$$\theta_3 = 0 \qquad\qquad \theta_3 = \pi \qquad\qquad \theta_3 = 2\pi$$

Figure 5. Schematic diagram showing a line segment (solid grey line) on $\mathbf{H}_B^{\mathrm{in}}$ (with $0 < r_3^a \leq r_3 \leq r_3^b < h$, shown in logarithmic polar coordinates) and its image (dashed grey line), after one cycle around the network. The length of the line segment is chosen such that its image covers the full range of values of θ_3. Note that in any particular example, the image could be considerably more complicated than a straight line.

In order to show this, we repeat part of the calculation of section 3.1 but starting on $\mathbf{H}_B^{\mathrm{in}}$ instead of $\mathbf{H}_A^{\mathrm{in}}$. For any given initial value of r_3 on $\mathbf{H}_B^{\mathrm{in}}$, using inequalities (17) and (21), the trajectory crosses $\mathbf{H}_A^{\mathrm{in}}$ with a value of $x_2^{(A_{\mathrm{in}})}$ that satisfies:

$$hD_{CA}^{\min}\left(\frac{r_3}{h}\right)^{\delta_B^{\max}\delta_C^{\max}} \leq x_2^{(A_{\mathrm{in}})}(r_3) \leq hD_{CA}^{\max}\left(\frac{r_3}{h}\right)^{\delta_B^{\min}\delta_C^{\min}}, \qquad (23)$$

where $D_{CA}^{\min} = D_A^{\min}\left(D_C^{\min}\right)^{\delta_C^{\max}}$ and $D_{CA}^{\max} = D_A^{\max}\left(D_C^{\max}\right)^{\delta_C^{\min}}$. On $\mathbf{H}_A^{\mathrm{in}}$, the trajectory has a value of $\theta_3^{(A_{\mathrm{in}})}$ close to that with which the unstable manifold of X crosses $\mathbf{H}_A^{\mathrm{in}}$, since we chose our initial line segment such that trajectories visited X. This is essentially a constant, but the complex eigenvalues mean that $\theta_3^{(A_{\mathrm{out}})}$ depends logarithmically on $x_2^{(A_{\mathrm{in}})}$. We want to choose r_3^a and r_3^b such that even allowing for the range of values of $x_2^{(A_{\mathrm{in}})}$ in (23), the local map (4) guarantees that the range of values of $\theta_3^{(A_{\mathrm{out}})}$ covers at least $[0, 2\pi]$. This requires that

$$\frac{\omega}{e_A}\log\left(\frac{\min\left(x_2^{(A_{\mathrm{in}})}(r_3^b)\right)}{\max\left(x_2^{(A_{\mathrm{in}})}(r_3^a)\right)}\right) > 2\pi,$$

where the minimum and maximum in this expression are taken over all possible

values of θ_3 on $\mathbf{H}_B^{\text{in}}$. This last expression can be rewritten as

$$\log\left(\frac{(r_3^b/h)^{\delta^{\max}}}{(r_3^a/h)^{\delta^{\min}}}\right) > \frac{2\pi c_A}{\omega} + \delta_A \log\left(\frac{D_{CA}^{\max}}{D_{CA}^{\min}}\right).$$

Values of r_3^a and r_3^b for which this is satisfied can clearly be found, regardless of the values of the global constants or the values of $\delta^{\min}$ and $\delta^{\max}$, provided that $\omega \neq 0$. Disregarding the global map constants ($D_{CA}^{\max}$ etc.), the inequality is satisfied if we choose $r_3^b > r_3^a \exp\left(2\pi c_A/\omega\delta^{\max}\right)$. By choosing r_3^a small enough (close enough to the network), the length of the initial line segment $r_3^b - r_3^a$ can be made as small as we wish.

With this choice of r_3^a and r_3^b, the line segment of initial conditions maps to at least a full circle on $\mathbf{H}_A^{\text{out}}$ and consequently, using the global map (13), also on $\mathbf{H}_B^{\text{in}}$, since that map rigidly rotates the angle. Therefore, on their next circuit around the network, trajectories from within this family could visit any of $\pm X$, $\pm Y$, $\pm P$ or $\pm Q$.

The same argument holds with minor changes regardless of the location of the initial line segment, so we conclude that close to the network, there are trajectories that visit any equilibrium point in C followed by any other equilibrium point in C on two consecutive circuits of the network. Since there is freedom in choosing the exact location of the line segment, this argument implies the same conclusion can be drawn for open sets of initial conditions. Thus we have shown that arbitrarily close to the network, there are open sets of orbits that switch from any route around the network to any other route.

The argument above does not require the network to be asymptotically stable, and only refers to two consecutive circuits of the network, and so does not demonstrate that typical trajectories will continue to switch for ever as they evolve. In the remainder of this section we consider long term switching, first in the case where the network is attracting ($\delta^{\min} > 1$) and then in the case where $\delta^{\min} < 1 < \delta^{\max}$.

The argument above implies that of trajectories starting in a typical ball of initial conditions close to the network and first visiting X, fewer than half will go on to visit X on their second circuit of the network. In the case $\delta^{\min} > 1$, all trajectories starting in a typical ball approach the network, so their values of $x_2^{(A_{\text{in}})}$ get smaller and smaller, and hence the values of $\theta_3^{(A_{\text{out}})}$ for these

24

trajectories get more and more spread out. Therefore, the argument that the chance of visiting X on the next cycle around the network is less than half continues to hold; in the limit, we expect that the set of trajectories that visit only X and never visit $-X$ has measure zero. Thus, typical trajectories should visit both $\pm X$ roughly equally, and there is always a chance they could visit $\pm Y$, $\pm P$ or $\pm Q$ as well.

We can estimate the probabilities of visiting different parts of the network by computing the proportion of trajectories starting on $\mathbf{H}_B^{\mathrm{in}}$ that will visit X or Y on their next time around the network. Consider a circle of initial conditions on $\mathbf{H}_B^{\mathrm{in}}$ with $r_3 = a$ $(a < h)$ and $0 \leq \theta_3 < 2\pi$. Of those in the first quadrant, some will visit X, some will visit P and the rest will visit Y (see Figure 4). The boundaries between the different possibilities are of the form $x_3 = K y_3^\alpha$, where $\alpha = e_{Bx}/e_{By} > 1$, and K is a constant that depends on which boundary is being considered. To simplify the discussion, we omit the details of those trajectories that visit P, and consider only a single boundary that separates trajectories that go via X and those that go via Y.

The intersection of the boundary with the circle $r_3 = a$ can be found by solving

$$a^2 = x_3^2 + y_3^2 = y_3^2 \left(1 + K^2 y_3^{2\alpha-2}\right)$$

for y_3 as a function of a, α and K. For small a and for $\alpha > 1$, the solution is approximately

$$y_3 = a \left(1 - \frac{1}{2} K^2 a^{2\alpha-2}\right), \qquad x_3 = K a^\alpha.$$

The proportion of trajectories starting on the circle $r_3 = a$ in $\mathbf{H}_B^{\mathrm{in}}$ that visit Y is approximately equal to $2x_3/2\pi a = K a^{\alpha-1}/\pi$ for small x_3. The same proportion visit $-Y$, and the remainder are split equally between X and $-X$.

In the case that the network is attracting $(\delta^{\min} > 1)$, the value of r_3 on $\mathbf{H}_B^{\mathrm{in}}$ decreases each time around the network, so $a \to 0$. Trajectories spend increasingly long periods of time near A, where the eigenvalues are complex, so one would expect that the angle θ_3 becomes essentially a random variable. In this case, the chance of visiting Y or $-Y$ goes to zero, and the chances of visiting X or $-X$ will both tend to $\frac{1}{2}$.

In the case $\delta^{\max} < 1$, where the network is unstable, trajectories leave the neighbourhood of the network and no estimates are possible.

The intermediate case ($\delta^{\min} < 1 < \delta^{\max}$) offers the interesting possibility that trajectories might maintain an average distance from the network, either in a periodic or chaotic fashion. In the latter case, one might expect that an average, weighted using the probabilities above, of the contraction around one part of the network and the expansion around the other part might lead to conditions for the existence of a nearby invariant set. Making a weighted average in this way only makes sense if trajectories switch *irregularly* between $\pm X$ and $\pm Y$, so an existence condition could include a requirement for switching. In the case of a periodic orbit, the weighting would depend on the itinerary of the orbit. This weighted average would also depend on a, which we interpret as the average distance from the network. We give numerical examples of this phenomenon below, and defer a detailed analysis of this case to a later paper.

4   Numerical example

In this section we present some numerical results based on the following equations:

$$
\begin{aligned}
\dot{x}_1 &= x_1(1 - x_1^2 - Ex_2^2), \\
\dot{x}_2 &= x_2(1 - x_2^2 - Fx_3^2 - Gy_3^2), \\
\dot{x}_3 &= x_3(1 - Ex_1^2 + Hx_2^2 - x_3^2 - Dy_3^2) - \omega y_3 x_1^2, \\
\dot{y}_3 &= y_3(1 - Ex_1^2 - Dx_3^2 - y_3^2) + \omega x_3 x_1^2,
\end{aligned}
\tag{24}
$$

where D, E, F, G and H are parameters that we vary in our numerics. The parameter H controls the relative values of the two expanding eigenvalues at the point B. Throughout we assume that $H > 0$, and that $D, E, F, G, (F + G)/(D + 1) \in (1, 3)$, so that assumptions **A1**–**A8** from section 2 are satisfied. The values of all parameters and eigenvalue ratios are given in Table 1.

To simplify the presentation, we always choose the parameter D so that δ_{CP} and δ_{CQ} are intermediate between δ_{CX} and δ_{CY}. With this constraint, the additional combinations of eigenvalue ratios are $\delta_C^{\max} = \max(\delta_{CX}, \delta_{CY})$, $\delta_C^{\min} = \min(\delta_{CX}, \delta_{CY})$. Recall that

$$
\delta_B^{\max} = \delta_{By}, \quad \delta_B^{\min} = \delta_{Bx}, \quad \delta^{\max} = \delta_A \delta_B^{\max} \delta_C^{\max}, \quad \delta^{\min} = \delta_A \delta_B^{\min} \delta_C^{\min}.
$$

26

Equilibrium point	Eigenvalues	Eigenvalue ratios
A: $(1,0,0,0)$	$r_A = 2$, $e_A = 1$, $c_A = E - 1$	$\delta_A = E - 1$
B: $(0,1,0,0)$	$r_B = 2$, $c_B = E - 1$, $e_{Bx} = 1 + H$, $e_{By} = 1$	$\delta_{Bx} = \frac{E-1}{1+H}$ $\delta_{By} = E - 1$
X: $(0,0,1,0)$	$r_C(\theta_3^X) = 2$, $\lambda_X = D - 1$, $e_C(\theta_3^X) = 1$, $c_C(\theta_3^X) = F - 1$	$\delta_{CX} = F - 1$
Y: $(0,0,0,1)$	$r_C(\theta_3^Y) = 2$, $\lambda_Y = D - 1$, $e_C(\theta_3^Y) = 1$, $c_C(\theta_3^Y) = G - 1$	$\delta_{CY} = G - 1$
P: $(0,0,\frac{1}{\sqrt{D+1}},\frac{1}{\sqrt{D+1}})$	$r_C(\theta_3^P) = 2$, $\lambda_P = 2\frac{D-1}{D+1}$, $e_C(\theta_3^P) = 1$, $c_C(\theta_3^P) = \frac{F+G}{D+1} - 1$	$\delta_{CP} = \frac{F+G}{D+1} - 1$
Q: $(0,0,-\frac{1}{\sqrt{D+1}},\frac{1}{\sqrt{D+1}})$	$r_C(\theta_3^Q) = 2$, $\lambda_Q = 2\frac{D-1}{D+1}$, $e_C(\theta_3^Q) = 1$, $c_C(\theta_3^Q) = \frac{F+G}{D+1} - 1$	$\delta_{CQ} = \frac{F+G}{D+1} - 1$

Table 1. Eigenvalues associated with equilibria of equations (24), and values of eigenvalue ratios. The actual eigenvalues at A (for example) are $-r_A$ (radial), $-c_A \pm i\omega$ (contracting) and e_A (expanding). The eigenvalues $-\lambda_X$, λ_P, $-\lambda_Y$ and λ_Q all have corresponding eigenvectors tangent to the invariant circle C.

Parameter	I	II	III
F	1.63125	1.63125	1.61875
G	1.671386719	1.549316406	1.671386719
$\delta_{Bx} = \delta_B^{\min}$	1.25	1.25	1.25
$\delta_{By} = \delta_B^{\max}$	1.28	1.28	1.28
δ_{CX}	0.63125	0.63125	0.61875
δ_{CY}	0.671386719	0.549316406	0.671386719
$\delta_{CP} = \delta_{CQ}$	0.63496867	0.57453782	0.62878055
δ_X	1.01	1.01	0.99
δ_Y	1.10	0.90	1.10
$\delta^{\max}$	1.10	1.0342400	1.10
$\delta^{\min}$	1.01	0.87890620	0.99

Table 2. Values of the parameters and the eigenvalue ratios for the three examples. The values in common are $\omega = 1$, $H = 0.024$, $D = 1.02$ and $E = 2.28$. The parameters F and G are set using $F = 1 + \delta_X (1 + H)/(E - 1)^2$ and $G = 1 + \delta_Y/(E - 1)^2$.

We make the further definitions $\delta_X = \delta_A \delta_{Bx} \delta_{CX}$ and $\delta_Y = \delta_A \delta_{By} \delta_{CY}$: these are the eigenvalue ratios relevant to trajectories that leave B along the x_3 (resp., y_3) direction and visit $\pm X$ (resp., $\pm Y$).

To illustrate typical dynamics near the network, we present three examples. In these examples, we choose values of δ close to 1 so that trajectories do not approach or leave the network too quickly. The first example has $\delta^{\min} > 1$, and the other two have $\delta^{\min} < 1 < \delta^{\max}$, with different choices as to whether it is δ_X or δ_Y that is less than 1. The specific choices of parameters and eigenvalue ratios for the different examples are given in Table 2.

- Example I: $\delta^{\min} = \delta_X = 1.01$ and $\delta^{\max} = \delta_Y = 1.10$. In this example, trajectories approach the network, predominantly switching between X and $-X$.
- Example II: $\delta^{\min} < \delta_Y = 0.90$ and $\delta^{\max} > \delta_X = 1.01$. In this case trajectories behave much as in Example I, even though the network is not asymptotically stable, since almost all trajectories visit $\pm X$ most of the time and so are most heavily influenced by the value of δ_X.
- Example III: $\delta^{\min} = \delta_X = 0.99$ and $\delta^{\max} = \delta_Y = 1.10$. Here trajectories leave a neighbourhood of the network and end up displaying periodic or chaotic switching.

Care needs to be taken with numerical integration of systems with heteroclinic cycles and networks, because of the potential for rounding errors to cause qualitatively incorrect results. We first integrated equations (24) numerically using the Bulirsch–Stoer adaptive integrator [32], with a tolerance for the relative error set to 10^{-12} for each step. We also rewrote equations (24) using logarithmic variables $(\log x_1, \log x_2, \log r_3, \theta_3)$ instead of (x_1, x_2, x_3, y_3), and integrated the converted equations with a tolerance of 10^{-10}, rising to 10^{-8} for trajectories very close to the network. This enabled us to examine whether the numerical methods handle the very large dynamic range of the variables without being unduly affected by rounding errors. The two methods of computing solutions agree to within the specified tolerance when we compute periodic trajectories (in calculations II and III), and they agree to within the specified tolerance for times up to about 3000 when we compute trajectories very close to the network. Beyond this time, trajectories computed by the two methods diverge, but the qualitative behaviour of the trajectories
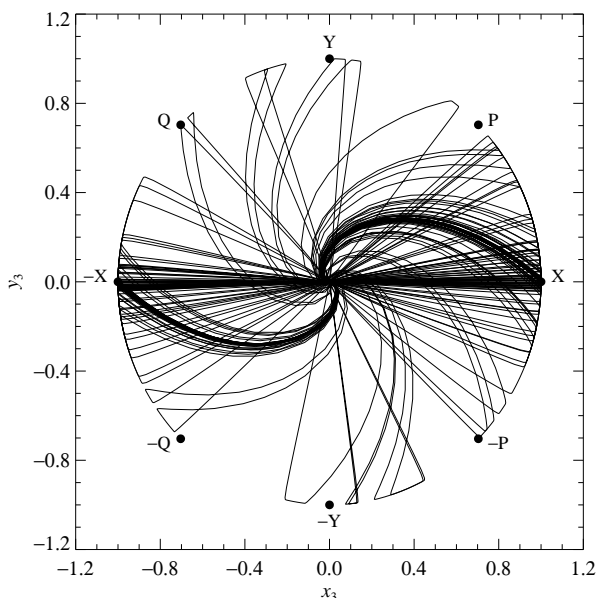
28

Figure 6.   Example I: Phase portrait showing the (x_3, y_3) projection of a single trajectory. The
trajectory leaves B (at the origin in this projection), goes to C (approximately the circle
$x_3^2 + y_3^2 = 1$) in a more-or-less straight line, travels around C towards $\pm X$ or $\pm Y$, then spirals in
to A (also at the origin) before returning to B.

is the same. We have confirmed that the results are not sensitive to the exact
value of the the relative error tolerance that we chose. The results shown in
the figures below are all computed using logarithmic variables.

Poincaré sections were computed using algorithms from [29]. The nodes
on the network are all simple equilibria lying within coordinate planes, so the
numerical issues associated with cycling chaos (chaotic dynamics within nodes
on the network), as discussed for example in [7, 11] do not arise here.

4.1   *Example I: Trajectories approach the stable network*

In this example, $\delta^{\min} = \delta_X = 1.01$ and $\delta^{\max} = \delta_Y = 1.10$ are both greater than
one, and the network is asymptotically stable. The phase portrait and time
series shown in Figures 6 and 7 correspond to a trajectory started from the
initial condition $x_1(0) = 0.01 = h$, $x_2(0) = 1$ and $x_3(0) = y_3(0) = 10^{-5}$, and
illustrate the occurrence of repeated switching in the transient dynamics. As
expected from section 3.2, a typical trajectory lying near the network makes
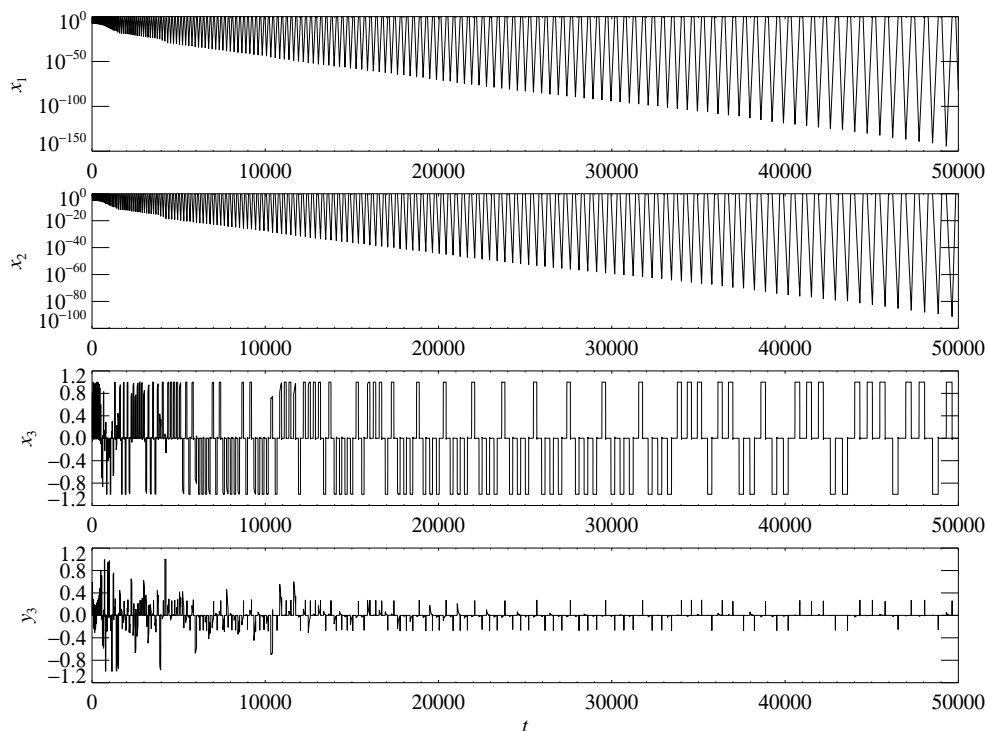
Figure 7.   Example I: Time series for the trajectory shown in Figure 6. The x_1 and x_2 plots show
that the trajectory is approaching the network. The x_3 plot shows the repeated switching
between X and $-X$, and the y_3 plot shows that visits to $\pm Y$ become increasingly rare as the
trajectory gets closer to the network.

repeated switches between X and $-X$ and visits $\pm Y$ occasionally, but the
visits to $\pm Y$ become increasingly rare as the trajectory gets closer to the
network.

Figure 8 shows where the trajectory intersects the Poincaré section $\mathbf{H}_B^{\mathrm{in}}$,
defined here as $x_1 = h = 0.01$, $x_2 \approx 1$ and $r_3 < h$. After leaving B, the
trajectory visits $\pm X$ or $\pm Y$: the symbols indicate which of the four possibilities
occurs immediately after the intersection marked. The boundaries separating
regions of $\mathbf{H}_B^{\mathrm{in}}$ from which trajectories leave for $\pm X$ and $\pm Y$ can be clearly
seen, and are consistent with the results sketched in Figure 5. As the trajectory
approaches the network, travelling from top to bottom in Figure 8, visits to $\pm Y$
are not seen for $r_3 < 10^{-20}$ or so, although they are in principle possible for
arbitrarily small r_3. Visits to X and $-X$ do not occur in a periodic fashion.
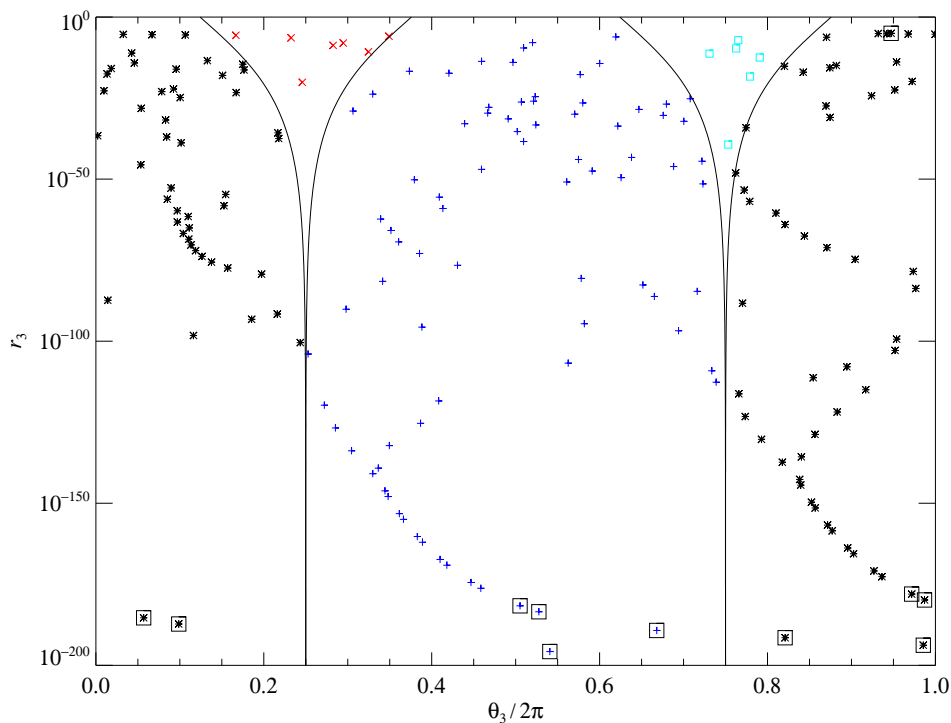
30

Figure 8.   Example I: Projection of a Poincaré section for the trajectory shown in Figure 6. Black asterixes (blue plusses) indicate that the trajectory visits X $(-X)$ immediately after leaving the Poincaré section; red crosses (cyan boxes) indicate that the trajectory next visits Y $(-Y)$. The single point in a box at the top is the first point in the trajectory, and the ten boxed points at the bottom are the final points. This figure illustrates how the trajectory approaches the network; the trajectory initially visits $\pm X$ and $\pm Y$, but as it approaches the network, visits to $\pm Y$ become rare while switching between X and $-X$ is persistent. The boundaries of the cuspoidal regions are indicative of the boundaries between trajectories that have different routes on their next circuit of the network (c.f., Figure 4). They have been chosen to match the available data for larger r_3.

4.2   *Example II: Trajectories approach the unstable network*

In this example, $\delta^{\min} < \delta_Y = 0.90$ and $\delta^{\max} > \delta_X = 1.01$, and the network is asymptotically unstable. However, trajectories that start close enough to the network can still approach the network. For instance, the initial condition $x_1(0) = 0.01 = h$, $x_2(0) = 1$, $x_3(0) = y_3(0) = 10^{-40}$ yields the trajectory shown in Figure 9 (below the horizontal line). This trajectory never visits $\pm Y$ but does switch repeatedly between X and $-X$ while getting closer to the network. In contrast, the initial condition $x_1(0) = 0.01 = h$, $x_2(0) = 1$, $x_3(0) = y_3(0) = 10^{-20}$ yields the periodic orbit close to the network shown above the
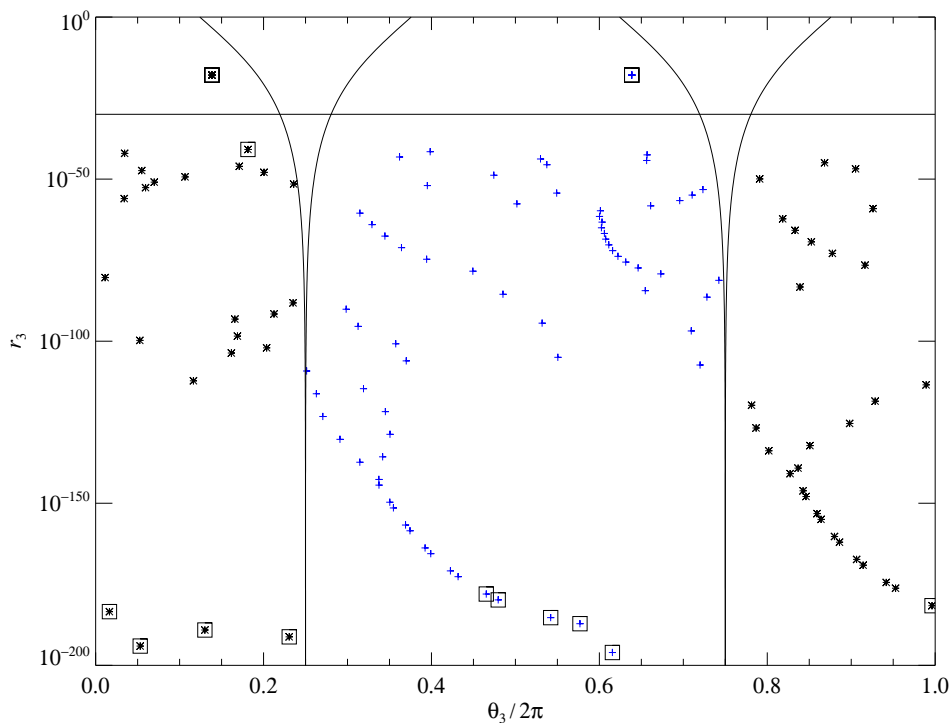
Figure 9.   Example II: Poincaré section. The trajectory with initial condition $x_1(0) = 0.01 = h$, $x_2(0) = 1$, $x_3(0) = y_3(0) = 10^{-40}$ (below the horizontal line) approaches the network, starting at the single boxed point just below the line, and ending at the ten boxed points at the bottom of the figure. The trajectory with initial condition $x_1(0) = 0.01 = h$, $x_2(0) = 1$, $x_3(0) = y_3(0) = 10^{-20}$ approaches a stable periodic orbit represented by the two boxed points above the line. Symbols are as in Figure 8.

horizontal line in Figure 9. There are other stable periodic orbits further away from the network.

This behaviour is consistent with the discussion in section 3. Since $\delta_X > 1$, a trajectory that starts close enough to the network will mostly only visit $\pm X$ (almost never $\pm Y$) and so can approach the network even if $\delta_Y < 1$. On the other hand, the discussion in section 3 predicts that there are trajectories arbitrarily close to the network that visit $\pm Y$ sufficiently often to be repelled from the network, and so the network is unstable. We have found examples of stable periodic orbits that are quite close to the network; most likely there are unstable periodic orbits as well, but we have not explored this possibility. We conjecture that the measure of initial conditions that do not eventually go to
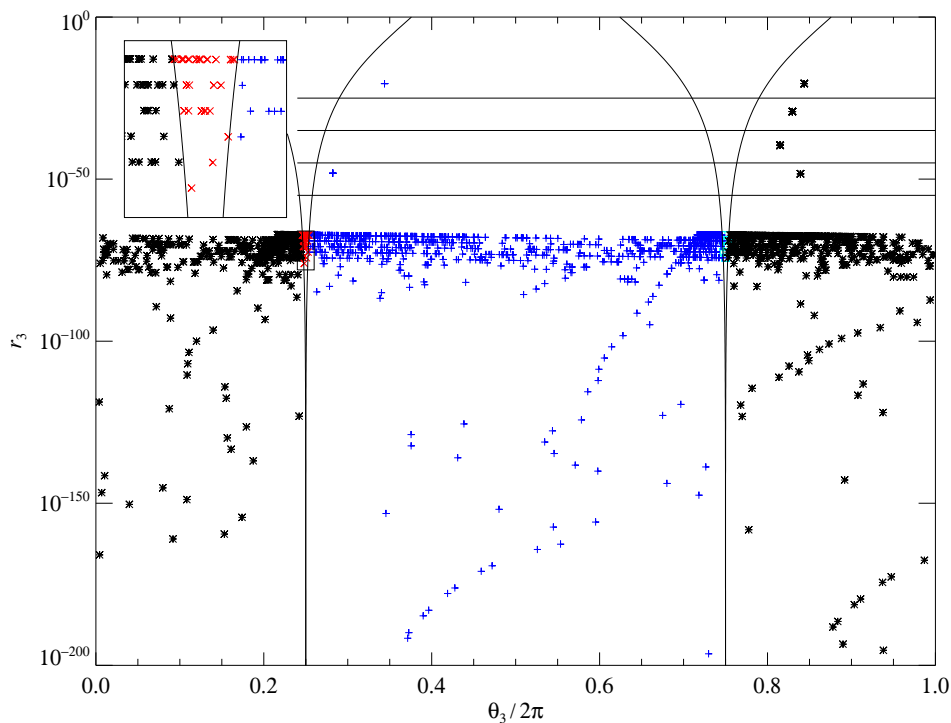
32

Figure 10.   Example III: Poincaré section, showing five trajectories separated by horizontal lines. With $x_1(0) = 0.01 = h$, $x_2(0) = 1$, $x_3(0) = y_3(0) = 10^{-200}$, the trajectory starts at the bottom of the figure and moves away from the network, but finds a chaotic attractor with $r_3 < 10^{-67}$ (below the lowest line). This trajectory chaotically switches between $\pm Y$ and $\pm X$. Above this, there are four examples of stable periodic orbits. The inset enlarges the boxed region near $\theta_3 = \pi/2$, $r_3 = 10^{-70}$. Symbols and colours are as in Figure 8.

the network tends to zero as these get closer to the network, so the network will be essentially asymptotically stable. The reason for this is that the cusps delimiting trajectories that go to $\pm Y$ (and all their preimages) are thin.

4.3   Example III: Trajectories leave the unstable network

The final example has $\delta^{\min} = \delta_X = 0.99$ and $\delta^{\max} = \delta_Y = 1.10$, and shows that although the network is unstable, there are nearby periodic and chaotic orbits. The Poincaré section in Figure 10 shows five trajectories. Each initially has $x_1(0) = 0.01 = h$ and $x_2(0) = 1$, and the x_3 and y_3 initial conditions vary between trajectories: from bottom to top in the figure, the initial conditions

are $x_3(0) = y_3(0) = 10^{-200}$, 10^{-50}, 10^{-40}, 10^{-30} and 10^{-20}, with the resulting trajectories being separated by horizontal lines in the figure. Trajectories starting with the four largest initial conditions find stable periodic orbits; there are most likely additional orbits that we have not found. In contrast, trajectories starting very close to the network move away and find a chaotic attractor at around $r_3 \approx 10^{-70}$. Within this attractor, the trajectory mostly visits $\pm X$ and moves gradually away from the network, since $\delta_X < 1$. As it does so, the chance of visiting $\pm Y$ increases; when this happens (with $\delta_Y > 1$), the trajectory jumps closer to the network. The same chaotic attractor was found with several initial conditions in the range $10^{-200} \le x_3(0) = y_3(0) \le 10^{-60}$. This example of sustained chaotic switching between $\pm X$ and $\pm Y$ illustrates the ideas discussed in section 3.2.

5   Conclusions

In this paper we have illustrated a simple mechanism that produces switching between different structurally stable heteroclinic cycles in a heteroclinic network, namely the presence of complex eigenvalues in the linearisation about one of the equilibria common to all cycles in the network. This is done in the context of an example in $\mathbb{R}^4$ with $\mathbb{Z}_2^3$ symmetry. Switching arising from the presence of complex eigenvalues has been seen in other examples [1, 2] but in those cases the cycles are structurally stable because of transversal intersections of some manifolds rather than purely because of the presence of symmetry.

By the construction and analysis of maps that model the dynamics near cycles in our network, we have found a simple condition under which the heteroclinic network is asymptotically stable. The construction of the maps used standard techniques that were modified to allow us to keep track of the continuum of heteroclinic cycles present in our network. A crucial step in the analysis of the network was recognition that the network could efficiently be treated as a collection of connections between equilibria (A and B) and an invariant circle (C) rather than a collection of cycles each of which connected a set of equilibria. Earlier attempts to treat the heteroclinic connections going to each of the equilibria on C (i.e., to $\pm X$, $\pm Y$, $\pm P$ and $\pm Q$) separately proved to be intractable and were ultimately unfruitful.

34

We found that the network is asymptotically stable if $\delta^{\min} > 1$. The quantity $\delta^{\min}$ was defined in section 3.1 and is the product of the ratios of the (real part of the) contracting and expanding eigenvalues at selected equilibria in the network, namely at A, B, and at the equilibrium on C at which the ratio of contracting to expanding eigenvalues is minimised. At B there are two expanding eigenvalues, and $\delta^{\min}$ is defined using the larger of these two eigenvalues. Effectively, $\delta^{\min}$ is the minimum ratio of contracting to expanding eigenvalues that could be encountered by a trajectory on one circuit through the network, starting and finishing at one of the common equilibria A or B.

Another important quantity for network stability is $\delta^{\max}$. As defined in section 3.1, $\delta^{\max}$ is effectively the maximum ratio of contracting to expanding eigenvalues that could be encountered by a trajectory on one circuit through the network. We showed that if $\delta^{\max} < 1$, then a trajectory started close to the network (but not on the stable manifold of any of the equilibria) will be further away from the network after one circuit of the network, regardless of its itinerary, and thus the network is unstable.

These results on network stability are a natural generalisation of established stability results for heteroclinic cycles, where it has been shown that asymptotic stability of a cycle is often determined (in part, at least) by the ratio of contracting to expanding eigenvalues along the cycle.

We have shown that switching is ubiquitous near our network. In particular, we showed that close enough to the network, there are trajectories that, over the course of two cycles around the network, visit any combination of the equilibrium points within C in any order. (A similar result holds for the examples of $[1, 2]$.) This occurs regardless of whether or not the network is asymptotically stable. In the case that the network is asymptotically stable, we showed that most trajectories repeatedly visit both X and $-X$ as they approach the network, while, on the assumption that the complex eigenvalues at A mix trajectories effectively, visits to $\pm Y$ become rare. Additive noise could clearly have an important effect on the switching behaviour; we have not explored this issue.

Our results about repeated switching in the network and our categorization of network stability in terms of $\delta^{\min}$ and $\delta^{\max}$ has allowed us to identify an interesting case, intermediate between asymptotic stability and complete instability of the network. Specifically, if $\delta^{\min} < 1 < \delta^{\max}$ then whether or not

an individual trajectory approaches the network or diverges from it depends on the detailed itinerary of that trajectory. We found two main cases. First, if the ratio of contracting to expanding eigenvalues encountered by a trajectory making a circuit near the dominant cycle in the network (i.e., a cycle involving a visit to either X or $-X$) is greater than one ($\delta_X > 1$, using the notation of section 4), then we conjecture that almost all trajectories will eventually converge to the network, even though the network is asymptotically unstable. If on the other hand, the dominant cycle has the appropriate ratio of eigenvalues less than one ($\delta_X < 1$) with one of the other cycles having a ratio greater than one ($\delta_Y > 1$, in the notation of section 4) then there might be a delicate balance between the repelling properties of the dominant cycle and the attracting properties of the other cycle; most trajectories would be repelled from the unstable network but may be attracted to a chaotic or periodic attractor some small distance away from the network. In this case, the network structure may still be observed in the long term dynamics of the system even though the network is unstable.

An example of this phenomenon was shown in section 4 where results from numerical integration of a particular system of differential equations were presented. We have not attempted to quantify the balance that occurs in the example of a chaotic attractor in section 4, but defer this to a later paper. We note that heteroclinic networks with delicate stability properties have been studied before (e.g., in [21]); the point of difference here is that the switching mechanism operating in our network ensures that most trajectories will visit most parts of a neighbourhood of the network. The transition from $\delta^{\min} > 1$ to $\delta^{\min} < 1$ is an example of a resonance of the heteroclinic network, and it is clear from this example that the network structure will make analysis of the resonance quite involved. We defer this analysis to a future paper.

Acknowledgments

36

Mathematics at Northwestern University, and the School of Mathematics at the University of Leeds.

References

[1] M. A. D. Aguiar, S. B. S. D. Castro, and I. S. Labouriau. Dynamics near a heteroclinic network. *Nonlinearity*, 18(1):391–414, January 2005.

[2] M. A. D. Aguiar, I. S. Labouriau, and A. A. P. Rodrigues. Switching near a network of rotating nodes. *Dyn. Syst. Int. J.*, 2009.

[3] D. Armbruster, E. Stone, and V. Kirk. Noisy heteroclinic networks. *Chaos*, 13(1):71–79, March 2003.

[4] P. Ashwin and J. Borresen. Discrete computation using a perturbed heteroclinic network. *Phys. Lett. A*, 347(4-6):208–214, December 2005.

[5] P. Ashwin and P. Chossat. Attractors for robust heteroclinic cycles with continua of connections. *J. Nonlin. Sci.*, 8(2):103–129, 1998.

[6] P. Ashwin and M. Field. Heteroclinic networks in coupled cell systems. *Arch. Rat. Mech. Anal.*, 148(2):107–143, 1999.

[7] P. Ashwin, M. Field, A. M. Rucklidge, and R. Sturman. Phase resetting effects for robust cycles between chaotic sets. *Chaos*, 13(3):973–981, September 2003.

[8] P. Ashwin, G. Orosz, J. Wordsworth, and S. Townley. Dynamics on networks of cluster states for globally coupled phase oscillators. *SIAM J. Appl. Dynam. Syst.*, 6(4):728–758, 2007.

[9] P. Ashwin and A. M. Rucklidge. Cycling chaos: its creation, persistence and loss of stability in a model of nonlinear magnetoconvection. *Physica D*, 122(1-4):134–154, November 1998.

[10] P. Ashwin, A. M. Rucklidge, and R. Sturman. Infinities of stable periodic orbits in systems of coupled oscillators. *Phys. Rev. E*, 66(3):art. no.–035201, September 2002.

[11] P. Ashwin, A. M. Rucklidge, and R. Sturman. Cycling chaotic attractors in two models for dynamics with invariant subspaces. *Chaos*, 14(3):571–582, September 2004.

[12] P. Ashwin, A. M. Rucklidge, and R. Sturman. Two-state intermittency near a symmetric interaction of saddle-node and Hopf bifurcations: a case study from dynamo theory. *Physica D*, 194(1-2):30–48, July 2004.

[13] W. Brannath. Heteroclinic networks on the tetrahedron. *Nonlinearity*, 7:1367–1384, 1994.

[14] F. H. Busse and K. E. Heikes. Convection in a rotating layer: A simple case of turbulence. *Science*, 208(4440):173–175, 1980.

[15] P. Chossat. Forced reflectional symmetry breaking of an $O(2)$-symmetric homoclinic cycle. *Nonlinearity*, 6(5):723–731, September 1993.

[16] P. Chossat, M. Krupa, I. Melbourne, and A. Scheel. Transverse bifurcations of homoclinic cycles. *Physica D*, 100(1-2):85–100, January 1997.

[17] R. Driesse and A. J. Homburg. Essentially asymptotically stable homoclinic networks. *Dyn. Syst. Int. J.*, 24:459–471, 2009.

[18] M. Field. *Lectures on Bifurcations, Dynamics and Symmetry*, volume 356 of *Pitman Research Notes in Mathematics*. Longman, 1996.

[19] J. Guckenheimer and P. Holmes. Structurally stable heteroclinic cycles. *Math. Proc. Camb. Phil. Soc.*, 103:189–192, January 1988.

[20] V. Kirk and A. M. Rucklidge. The effect of symmetry breaking on the dynamics near a structurally stable heteroclinic cycle between equilibria and a periodic orbit. *Dyn. Syst. Int. J.*, 23(1):43–74, March 2008.

[21] V. Kirk and M. Silber. A competition between heteroclinic cycles. *Nonlinearity*, 7(6):1605–1621, November 1994.

[22] M. Krupa and I. Melbourne. Asymptotic stability of heteroclinic cycles in systems with symmetry. *Ergod. Theory Dyn. Syst.*, 15:121–147, February 1995.

[23] M. Krupa and I. Melbourne. Nonasymptotically stable attractors in $O(2)$ mode interactions. In W. Langford and W. Nagata, editors, *Normal Forms and Homoclinic Chaos*, volume 4 of *Fields Institute Communications*, pages 219–232, Providence, RI, 1995. Amer. Math. Soc.

[24] M. Krupa and I. Melbourne. Asymptotic stability of heteroclinic cycles in systems with symmetry. II. *Proc. Roy. Soc. Edin. A*, 134:1177–1197, 2004.

[25] I. Melbourne. Intermittency as a codimension-three phenomenon. *J. Dyn. Stab. Sys.*, 1:347–367, 1989.

[26] I. Melbourne. An example of a non-asymptotically stable attractor. *Nonlinearity*, 4(3):835–844, August 1991.

[27] I. Melbourne, M. R. E. Proctor, and A. M. Rucklidge. A heteroclinic model of geodynamo reversals and excursions. In P. Chossat, D. Armbruster, and I. Oprea, editors, *Dynamo and Dynamics, a Mathematical Challenge*, pages 363–370., Dordrecht, 2001. Kluwer.

[28] C. Nore, F. Moisy, and L. Quartier. Experimental observation of near-heteroclinic cycles in the von Kármán swirling flow. *Phys. Fluids*, 17:064103, 2005.

[29] T. S. Parker and L. O. Chua. *Practical Numerical Algorithms for Chaotic Systems*. Springer, New York, 1989.

[30] C. M. Postlethwaite and J. H. P. Dawes. Regular and irregular cycling near a heteroclinic network. *Nonlinearity*, 18(4):1477–1509, July 2005.

[31] C. M. Postlethwaite and J. H. P. Dawes. A codimension-two resonant bifurcation from a heteroclinic cycle with complex eigenvalues. *Dyn. Syst. Int. J.*, 21(3):313–336, September 2006.

[32] W. H. Press, B. P. Flannery, S. A. Teukolsky, and W. T. Vetterling. *Numerical Recipes – the Art of Scientific Computing*. Cambridge University Press, Cambridge, 1986.

[33] A. M. Rucklidge. Global bifurcations in the Takens–Bogdanov normal form with D_4 symmetry near the $O(2)$ limit. *Phys. Lett. A*, 284(2-3):99–111, June 2001.

[34] B. Sandstede and A. Scheel. Forced symmetry breaking of homoclinic cycles. *Nonlinearity*, 8(3):333–365, May 1995.

[35] A. Scheel and P. Chossat. Bifurcation d'orbites périodiques à partir d'un cycle homocline symétrique. *C. R. Acad. Sci. Paris Ser. I*, 314:49–54, 1992.

[36] E. Stone and P. Holmes. Random perturbations of heteroclinic attractors. *SIAM J. Appl. Math*, 50(3):726–743, June 1990.